Phenotypic Characteristics Including In Vivo Cone Photoreceptor Mosaic in *KCNV2*-Related "Cone Dystrophy with Supernormal Rod Electroretinogram"

Ajoy Vincent,[1,2] *Tom Wright,*[1] *Yaiza Garcia-Sanchez,*[1] *Marsha Kisilak,*[3,4] *Melanie Campbell,*[3,4] *Carol Westall,*[1,2] *and Elise Héon*[1,2,5]

Purpose. To report phenotypic characteristics including macular cone photoreceptor morphology in *KCNV2*-related "cone dystrophy with supernormal rod electroretinogram" (CDSR).

Methods. Seven patients, aged 9 to 18 years at last visit, with characteristic full-field electroretinographic (ERG) features of CDSR were screened for mutations in the *KCNV2* gene. All patients underwent detailed ophthalmological evaluation, which included distance and color vision testing, contrast sensitivity measurement, fundus photography, fundus autofluorescence (FAF) imaging, and spectral domain-optical coherence tomography (SD-OCT). Follow-up visits were available in six cases. Rod photoreceptor function was assessed using a bright white flash ERG protocol (240 cd·s/m^2). Macular cone photoreceptor morphology was assessed from 2° by 2° zonal images obtained using adaptive optics scanning laser ophthalmoscopy (AOSLO) in six cases.

Results. Pathogenic mutations in *KCNV2* were identified in all seven cases. Best corrected vision was 20/125 or worse in all cases at the latest visit (20/125–20/400). Vision loss was progressive in two cases. Color vision and contrast sensitivity was abnormal in all cases. Retinal exam revealed minimal pigment epithelial changes at the fovea in four cases. A peri- or parafoveal ring of hyperfluorescence was the most common FAF abnormality noted (five cases). The SD-OCT showed outer retinal abnormalities in all cases. The rod photoreceptor maximal response was reduced but rod sensitivity was normal. AOSLO showed markedly reduced cone density in all six patients tested.

Conclusions. Central vision parameters progressively worsen in CDSR. Structural retinal and lipofuscin accumulation abnormalities are commonly present. Macular cone photoreceptor mosaic is markedly disrupted early in the disease. (*Invest Ophthalmol Vis Sci.* 2013;54:898–908) DOI:10.1167/iovs.12-10971

"Cone dystrophy with supernormal rod electroretinogram" (CDSR) is an autosomal recessive disorder first described by Gouras et al. in 1983.[1] Affected individuals usually present within the first two decades of life with symptoms of diminution of distant vision and photophobia; a history of nyctalopia is present in about 50% of cases.[2–5] Nystagmus is observed in a subset of cases, but is more common in children.[6] Color vision deficits, myopia, and central scotoma are commonly described.[2,4,5,7] Fundus findings are usually unremarkable in children, but adults frequently show macular retinal pigment epithelial (RPE) changes or atrophy.[1–8]

The nomenclature "CDSR" has its origin from the unique full-field electroretinogram (ERG) characteristics found in the disease[1] and is summarized here. The scotopic ERG to dim-light stimulus ($\leq$0.01 cd·s/m^2) is either nondetectable or markedly subnormal and delayed. With further small increments in stimulus luminance, disproportionate large increments are noted in the rod b-wave amplitude that attains high-normal or supernormal values at Standard flash (3.0 cd·s/m^2).[5] At flash strengths $\geq$3.0 cd·s/m^2, the rod a-wave shows late squaring.[5] The cone ERGs are reduced and delayed. There is evidence from electrophysiological tests that suggests the locus of abnormality to be post-phototransduction.[9]

Wu et al.[10] identified mutations in *KCNV2*, a gene encoding the voltage-gated K^+ channel subunit to cause this disorder. *KCNV2* encodes for a 545 amino acid protein structurally composed of an N-terminal A and B box, six transmembrane domains (S1–S6), and a pore loop (between S5 and S6).[11,12] KCNV2 forms functional hetero-tetramers with other K^+ channel subunits like KCNB1, KCNC1, and KCNF1.[11,13] Since only mutations in *KCNV2* have been associated with CDSR, recognition of the pathognomonic ERG features helps to direct mutational analysis.

Although the diagnostic features of CDSR are found in rod-derived ERGs, the functional abnormalities observed in affected individuals are predominantly a result of macular cone involvement, which slowly worsens over time.[5] Adaptive optics scanning laser ophthalmoscopy (AOSLO) and spectral-domain optical coherence tomography (SD-OCT) are complementary high resolution retinal imaging techniques that enable excellent lateral[14–19] and axial resolution,[20,21] respectively. The

From the [1]Department of Ophthalmology and Vision Sciences, The Hospital for Sick Children, Toronto, Canada; the [2]Department of Ophthalmology and Vision Sciences, University of Toronto, Canada; the [3]Department of Physics and Astronomy, University of Waterloo, Waterloo, Ontario, Canada; the [4]School of Optometry and Vision Science, University of Waterloo, Waterloo, Ontario, Canada; and the [5]Department of Genetics and Genome Biology, The Hospital for Sick Children, Toronto, Canada.

Part of this work was presented at the International Symposium on Retinal Degeneration in Bad Gogging, Bavaria, Germany, July 2012.

Supported by the Mira Godard research fund (EH), Canadian Foundation for Innovation (CW, MC), Natural Sciences and Engineering Research Council of Canada (MC, CW), and Canadian Institute of Health Research (CW, MC).

Submitted for publication September 15, 2012; revised November 16, 2012; accepted December 2, 2012.

Disclosure: **A. Vincent**, None; **T. Wright**, None; **Y. Garcia-Sanchez**, None; **M. Kisilak**, None; **M. Campbell**, None; **C. Westall**, None; **E. Héon**, None

Corresponding author: Elise Héon, Department of Ophthalmology and Vision Sciences, The Hospital for Sick Children, 555 University Avenue, Toronto, Canada, M5G 1X8; eheon@attglobal.net.

Investigative Ophthalmology & Visual Science, January 2013, Vol. 54, No. 1

AOSLO allows visualization of individual photoreceptors; SD-OCT allows retinal depth resolution of 3 to 5 μm. Studies on cone mosaic and density, and their relation to photoreceptor layer architecture in certain cone dysfunction syndromes and retinal dystrophies have recently appeared.[22–27] SD-OCT shows outer retinal abnormalities in CDSR.[28] The current study details phenotypic characteristics of CDSR, including an in-depth examination of rod-derived ERG components, and describes, for the first time, macular cone photoreceptor morphology in *KCNV2*-related disease.

Methods

The study followed the tenets of the Declaration of Helsinki and was approved by the Ethical Review Board at The Hospital for Sick Children, Toronto. Seven participants (cases 3 and 4 are siblings) with characteristic ERG changes of CDSR were recruited. The age at first visit ranged from 2 to 16 years.

Clinical Assessment, Autofluorescence Imaging, OCT, and Visual Field Analysis

A comprehensive history and detailed eye examination, which included assessments of best corrected visual acuity (BCVA), color vision (Hardy Rand Rittler charts), contrast sensitivity (Pelli Robson charts), and fundus were performed in all cases. Follow-up visits were available in all except case 6. Fundus autofluorescence (FAF) testing was done in all cases (Visucam$^{NM/FA}$; Carl Zeiss Meditec, Jena, Germany). Spectral-domain OCT imaging (Cirrus; Carl Zeiss Meditec) included acquisition of five line horizontal raster scans centered at the fovea (6-mm length, 0.25-mm spacing, and 4096 A-scans per B-scan) in all cases. Additional five-line raster scans at a different orientation or location were performed when needed. Macular volume scans (cube scan: 6 by 6 mm, 128 horizontal scans comprising 1024 A-scans each) were acquired; central subfoveal thickness (between RPE and internal limiting membrane) and average macular cube thickness (calculated by inbuilt software) were compared with age-matched control participants. Goldmann visual field perimetry was done in four cases using I4e and III4e targets (cases 1, 2, 5, and 6).

Electroretinography

Extended full-field ERG testing largely based on the latest International Society for Clinical Electrophysiology of Vision Standards[29] or similar[30] was performed in all seven cases using Burian-Allen electrodes. As such, stimulus strengths for eliciting ERG responses (in cd·s/m^2) are specified alongside each testing parameter. After 20-minute dark adaptation (DA), dim-light scotopic response (DA0.002 ERG) and combined rod–cone response (DA2.29 ERG) were recorded. A bright flash ERG (DA7.6 ERG) was performed in all cases except case 6. Additional DA ERGs were available: DA0.0004 (all cases), DA0.001 (cases 1, 3, 5, 6, 7), DA0.006 (all cases), and DA0.016 (case 2). After 10-minute light adaptation (LA), a single flash photopic response (LA2.29 ERG) and a 30-Hz flicker (LA2.29 30 Hz ERG) were recorded. In case 6, ERG was recorded in the operating room under sevofluorane anesthesia following 20 minutes of dark adaptation; the results were compared to control ERGs obtained under similar conditions. Follow-up ERGs were obtained in cases 1, 3, 4, 5, and 7.

Rod photoreceptor function was evaluated further in all cases. A scotopic ERG recording was obtained using a white flash of high luminance (240 cd/·/m^2; DA240 ERG). The cone contribution to the DA240 ERG was deduced by recording a photopic ERG using the same flash strength (LA240 ERG; 30 cd/m^2 background) following light adaptation. The rod photoreceptor function was derived by digitally subtracting the LA240 ERG from the DA240 ERG as previously described.[31,32] Rod photoreceptor maximal response amplitude (A_{max}) was derived by fitting a horizontal line at the beginning of squaring of the subtracted response (amplitude measured from baseline).[31–33] The sensitivity of rod photoreceptor function was calculated from a slope fitted to the steepest part of the derived a-wave (within 10 ms) and measuring the timing of the intercept with the maximal amplitude (t_{Amax}).[9,31–33] The t_{Amax} and A_{max} were compared with age-matched controls.

Adaptive Optics Scanning Laser Ophthalmoscopy Imaging

Retinal images from at least one eye were captured using an adaptive optics enhanced confocal scanning laser ophthalmoscope (AOSLO; multi-modal AO System; Physical Sciences Inc., Andover, MA) following cycloplegia and pupillary dilatation in six cases (except case 1). Retinal fields (2° by 2°) were imaged in AOSLO mode with a 760-nm scanning laser. A Hartman-Shack wavefront sensor measured optical aberrations induced by the passage of light through the eye's optics; the measured aberrations were then corrected using a 97-element deformable mirror (Hi-Speed DM97-15; Alpao, Giéres, France). High spherical refractive errors were corrected using an appropriate supplementary lens inserted into the system at a pupil plane. The image returning from the eye was recorded as a movie using 1024 by 1000 pixels per frame at 24 frames per second. A minimum of 100 frames were recorded at each retinal location; multiple videos were taken within a 6° eccentricity of the fovea along the horizontal axis. Fixation and retinal location were monitored using a low-resolution fundus image captured simultaneously with the AOSLO movie. The AOSLO movies were postprocessed by contrast enhancing, aligning, and averaging three consecutive frames manually chosen to have the best brightness and focus, except in case 5 in which 10 consecutive frames were averaged.[34] In cases, approximate locations of the averaged AOSLO images were determined from blood vessel markings in the low-resolution fundus image and color fundus photographs. Due to the presence of nystagmus, marking of the retinal locus in cases 3, 4, 5, and 7 was approximate. Due to the grossly abnormal cone mosaics, manual counting was performed independently by two people only in cases 2, 3, and 4, using the cell counter plug-in for ImageJ software.[35] Cone density was calculated over subregions selected for best focus in the averaged 2° by 2° frame; multiple averaged frames from same locus were counted. Counts were converted to density measures in square millimeters by using measured axial eye lengths.

Genetic Testing

Genomic DNA was extracted from peripheral blood in all seven cases. The two coding exons and intron–exon boundaries of *KCNV2* were amplified by polymerase chain reaction (PCR: Héon lab) using custom-designed primer pairs. Direct sequencing of PCR products was performed at McGill University and Génome Québec Innovation Centre, Montréal. Segregation analysis was performed in four families. Allele frequency of novel changes was tested in 300 control chromosomes by amplification refractory mutation system assay or restriction enzyme digest (details available on request).

Statistical Testing

Unpaired *t*-tests were performed on data obtained from the right eye of cases ($n = 7$) and age-matched controls ($n = 20$) for SD-OCT and rod receptor function parameters. Sidak corrected *P* values were used to ascertain significance in multiple comparisons.

Results

Clinical Phenotype

The salient clinical features in the seven cases are summarized in Tables 1 and 2. The mean follow-up period in six cases was 7.5 years (median = 9 years, follow-up interval = 2–11 years). A

Table 1. Clinical Characteristics in the Seven Cases

Case/Sex	Age, y	Salient History, Symptoms, and Signs	BCVA RE:LE	Refraction RE:LE	Color Vision BE	CS (RE:LE)
1/M	8	Minimal nystagmus since infancy; diminution of vision for 2 y; no nyctalopia; mild hemeralopia; head shaking present	20/60:20/100	+2.0 DSph/+1.0 DCyl x 115°: +2.75 DSph/+1.25 DCyl x 70°	Moderate RG deficit, severe BY deficit	1.35:1.05
	11	Micronystagmus; head shaking absent	20/200:20/125	Same as above	Severe RG and BY deficits	1.05:1.05
2/M	16	Nystagmus since infancy that improved; diminution of vision for 10 y; Photophobia for 15 y; Takes time to adjust to dimly lit conditions	20/70:20/200	−3.50 DSph/+0.75 DCyl x 60°: Plano/+0.50 DCyl x 120°	Severe RG and BY deficits	1.05:1.05
	18	No change in symptoms noted	20/200:20/200	Same as above	Severe RG and BY deficits	1.05:1.05
3/M	4	Diminution of vision; horizontal nystagmus; right esotropia 20 PD	20/200:20/200	−5.50 DSph: −6.75 DSph	Not tested	Not tested
	15	Improvement in nystagmus; nyctalopia for 12 y; photophobia for 9 y	20/200:20/200	−9.0 DSph/+1.75 DCyl x 90°: −10.25 DSph/+1.0 DCyl x 90°	Severe RG and BY deficits	1.05:1.05
4/M	2	Asymptomatic	CSM	+0.25 DSph: +1.00 DSph	Not tested	Not tested
	13	Nyctalopia for 9 y; photophobia for 4 y; micronystagmus	20/125:20/200	−7.0 DSph: −6.25 DSph	Protan and tritan deficits (large D15)	1.20:1.20
5/M	4	Horizontal nystagmus for 4 y; head shaking for 1 y; diminution of distant vision	20/200:20/200	+1.50 DSph: +2.00 DSph	Not tested	1.20:1.20
	11	Nystagmus improved; photophobia for 7 y; nyctalopia for 3 y; head shaking better	20/200:20/200	Same as above	Severe RG deficit, moderate BY deficit	1.20:1.20
6/M	9	No nystagmus; Mild nyctalopia for 5 y; photophobia for 5 y	20/125:20/200	−7.0 DSph/+1.0 DCyl x 130°: −6.75 DSph	Severe RG deficit, moderate BY deficit	1.05:1.05
7/F	6	Nyctalopia and photophobia; micronystagmus; alternate exotropia 20 PD	20/200:20/200	−2.5 DSph: −3.5 DSph	Not tested	Not tested
	10	No worsening of symptoms	20/200:20/200	−4.0 DSph/−1.00 DCyl x 180°; −4.75 DSph/−0.75 DCyl x 180°	Severe RG deficit, moderate BY deficit	0.45:0.45
	17	Worsening of distance vision	20/400:20/400	Same as above	Not tested	0.45:0.45

RE, right eye; LE, left eye; BE, both eyes; RG, red–green; BY, blue–yellow; CS, contrast sensitivity; CSM, central steady maintenance; PD, prism diopters.

history of nystagmus since early childhood or presence of micronystagmus on evaluation, or both was present in six of the seven cases. The amplitude of the nystagmus improved in three cases (cases 2, 3, and 5). Photophobia was observed in all seven cases. Nyctalopia or a delay in adjusting to a dimly lit environment was noted in six cases. Head shaking was observed in two cases initially (cases 1 and 5), but this spontaneously resolved in case 1 by 11 years. A myopic refractive error was noted in five cases. The BCVA at distance was 20/125 or worse in all eyes at the latest visit (range: 20/125–20/400; age range: 9–18 years). Cases 1 and 2 showed progressive visual loss ($\geq$2 lines) in at least one eye. Color vision testing showed abnormalities in both red–green and blue–yellow axes in all eyes. Contrast sensitivity was also reduced in all eyes at last visit (range: 0.45–1.20 log units). The only notable retinal findings were either a dull foveal reflex (three cases: aged 11–17 years) or mild macular RPE changes (four cases: aged 9–18 years; Figs. 1A–G). On FAF imaging, a perifoveal ring of hyperfluorescence was noted in five cases (Figs. 1H, 1J–L, and 1N); a nonspecific pattern of foveal or perifoveal hyperfluorescence was seen in the other two (Figs. 1I, 1M).

The SD-OCT showed some disruption of the photoreceptor inner segment–outer segment (IS-OS) junction and underlying outer segment (OS) layer at the fovea in all 14 eyes (Figs. 1O–V). In case 3 (15 years), disruption of IS-OS junction and OS was complete such that neither layer was discernible (Fig. 1R); whereas, in cases 6 and 7, an optical gap (hyporeflective region) was seen to replace the IS-OS junction and OS completely (Figs. 1U, 1V). Case 6 also had persistent inner retinal layers at the fovea consistent with foveal hypoplasia. The RPE, Bruchs membrane, and the external limiting membrane were reasonably preserved in all cases. The mean central subfoveal thickness was reduced in the cases (cases = 181.6 $\pm$ 17.6 μm; control participants: 243.5 $\pm$ 12.8 μm; $P < 0.001$). The average retinal thickness within the macular cube was also reduced in the cases (cases = 250.3 $\pm$ 10.0 μm; control participants: 276.9 $\pm$ 12.7 μm; $P < 0.001$). Table 2 details SD-OCT findings in all seven cases.

Table 2. Retinal Findings in the Cases at the Most Recent Visit

Case/ Age	Macular Fundus Appearance	Autofluorescence	Optical Coherence Tomography Findings RE:LE*
1/11	Dull foveal reflex	Faint perifoveal hyperfluorescent ring	Disruption of photoreceptor IS-OS junction and photoreceptor OS at the fovea; CST, 175:172 μm; CAT, 264:265 μm
2/18	Minimal RPE changes	Hyperfluorescence at perifoveal region	Disruption of photoreceptor IS-OS junction and OS at the fovea; CST, 168:170 μm; CAT, 250:244 μm
3/15	Minimal RPE changes	Broad parafoveal ring of hyperfluorescence with central RPE atrophy	Complete disruption of photoreceptor IS-OS junction and OS at the fovea; CST, 162:166 μm; CAT, 251:247 μm
4/13	Dull foveal reflex	Faint perifoveal hyperfluorescent ring	Presence of all layers at fovea, mild disruption of photoreceptor IS-OS junction at fovea; CST, 211:204 μm; CAT, 260:274 μm
5/11	Minimal RPE changes	Faint perifoveal hyperfluorescent ring	Early disruption of photoreceptor IS-OS junction and OS layer at the fovea; CST, 185:NA; CAT, 251:NA
6/9	Minimal RPE changes	Faint hyperfluorescence at the fovea	Optical gap at the fovea, disruption of photoreceptor IS-OS junction and photoreceptor OS at fovea, presence of inner retinal layers at foveola; CST, 198:198 μm; CAT, 240:248 μm
7/17	Dull foveal reflex	Perifoveal ring of hyperfluorescence	Optical gap at the fovea, disruption of photoreceptor IS-OS junction and photoreceptor OS at fovea; CST, 172:185 μm; CAT, 236:233 μm

Age, age at testing; CST, central subfield thickness; CAT, cube average thickness; NA, not available.
* The CST in all cases were thinner (>2 SD) than in control participants.

Goldmann visual field testing was normal in case 1 (11 years). Case 2 demonstrated a small central scotoma (5° and 15° in the right and left eyes, respectively) to the I4e target at 16 years, which enlarged to involve 30° in either eye at 18 years. Case 6 also had a central 25° scotoma to the I4e target at 9 years; case 5 at 12 years had a few early scotomas in the central 10° field to I4e target (data not shown).

Electrophysiology Phenotype

Figure 2 details the ERG phenotype in three representative cases. The DA0.002 ERG b-wave was nonrecordable in four subjects (cases 3–6). Cases 1, 2, and 7 had markedly delayed DA0.002 ERG b-wave peak time; case 2 had subnormal b-wave amplitude. The DA2.29 ERG a-wave in all eyes demonstrated a normal a-wave slope initially, which plateaued suddenly, thus giving the appearance of a late squaring of the waveform. The DA2.29 ERG a-wave amplitudes were normal in all cases. The DA2.29 ERG b-wave onset and peak time were delayed in all cases. The DA2.29 ERG b-wave amplitude was supernormal or high normal in six cases; in case 6 (sevofluorane anesthesia), the ERG b-wave was within normal range for matched conditions. The DA7.6 ERG a- and b-wave showed characteristics similar to those obtained with DA2.29 stimulus in all six cases tested; the late alteration of the slope and squaring of the a-wave were more evident at this higher intensity. Rod responses obtained at various luminance (from 0.0004 to 2.29 cd·s/m^2) showed disproportionate large increments in b-wave amplitude with relatively small increments in flash luminance in cases 1 and 2 (Fig. 3). Four other cases (except case 6) that had subnormal rod b-wave amplitudes until DA0.002 stimulus intensity, had high/supernormal rod b-waves at DA2.29 stimulus intensity (Fig. 3).

The LA2.29 ERG a-wave was delayed in all cases; the a-wave amplitude was subnormal in five cases (cases 1, 4, 5, 6, and 7) and was at the lower limits of normal in the other two. The b-wave of LA2.29 single flash and 30-Hz flicker responses were delayed and subnormal in all seven cases. There was no progression of the ERG parameters on follow-up testing (five cases; range 1–8 years; mean 6.75 years between measurements).

The sensitivity of the rod photoreceptor function was normal in cases. The mean t_{Amax} (digitally subtracted response) in the cases was 9.0 ± 2.01 ms, not different from control participants (7.99 ± 0.96 ms; $P = 0.36$). But the mean A_{max} was reduced in cases (cases = −190.6 ± 48.4 μV; control participants = −330.9 ± 104.4 μV; $P = 0.005$). Notably, cases 5 and 7 had a markedly reduced A_{max} compared with the other cases (−149 μV: 11 years and −101 μV: 17 years, respectively). The squaring of the a-wave was clearly evident in the derived response.

Adaptive Optics Scanning Laser Ophthalmoscopy Imaging

The cone photoreceptor mosaic was disrupted and the cone density was reduced in all six cases tested (cases 2–7; Figs. 4A–G). Individual or groupings of cones, surrounded by patches of absent or non–wave-guiding cones, were seen in all cases. Case 2 had the highest measured cone density (4145 cones/mm^2; Fig. 4A; image centered 1.0° temporal to fovea). Case 3 had a cone density ranging across frames from 1329 to 1528 cones/mm^2 (Fig. 4B; centered 3.8° temporal to the fovea); cone density in case 4 ranged between 497 and 817 cones/mm^2 (Fig. 4C; centered 5.2° temporal to the fovea). In case 5 (Fig. 4D; centered 1.7° temporal to the fovea), case 6 (Fig. 4E; centered 0.2° nasal to fovea), and case 7 (Figs. 4F, 4G; centered 0° and 4.0° temporal to the fovea, respectively), cone mosaics were far more disrupted and counts were not performed. Cone mosaic obtained from a 25-year-old control subject at similar eccentricities is shown (Figs. 4H–J); cone densities at similar eccentricities were 13,302 cones/mm^2 (∼2.3° temporal to fovea) and 11,360 cones/mm^2 (∼4.8° temporal to fovea), respectively. The resolution of the AOSLO system used does not allow reliable resolution of cones in normal eyes within the central degree (Fig. 4H).

Sections of SD-OCT (2°) that overlap the horizontal meridian scanned by AOSLO are also shown in Figure 4. In cases 2, 6 and 7 (Figs. 4A, 4E, 4F), part of the AOSLO and corresponding SD-OCT images are within 1° of the fovea. In cases 6 and 7, the horizontal and vertical SD-OCT raster scans suggested the presence of an optical gap (hyporeflective region) in the photoreceptor OS about the fovea occupying 250 and 500 μm, respectively (∼0.75° and ∼1.5°, respectively). The AOSLO images from the corresponding regions show wide areas of absence of cones in both cases (Figs. 4E, 4F). In case 2, the SD-OCT raster scans show less disruption of the IS-OS junction and OS at 250 μm from the fovea (Fig. 1Q) compared

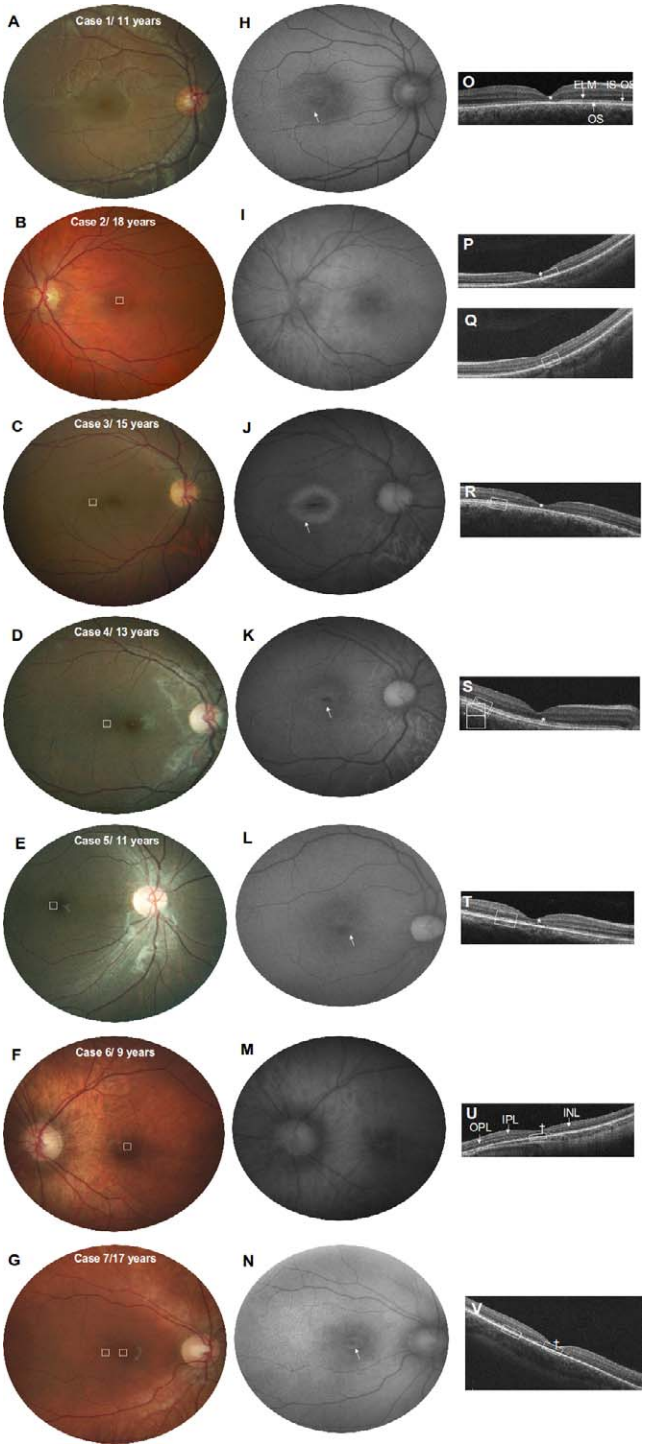

Figure 1. Fundus photographs (**A–G**), FAF images (**H–N**), and SD-OCT images (**O–V**) from one eye of all seven cases. Each *horizontal panel* represents corresponding fundus photo and FAF and SD-OCT images from the same eye of each individual case. Fundus photos show minimal retinal pigment epithelial changes at the macula in cases 2, 3, 6, and 7 (**B**, **C**, **F**, **G**). *White boxes* in fundus images represent 2° by 2° retinal locations from where AOSLO images were obtained. FAF showed a perifoveal ring of hyperfluorescence in five cases (*white arrows* in **H**, **J–L**, **N**). The SD-OCT (**O–V**) images show disruption of the IS-OS junction (*asterisk*) or optical gap (*cross*) at the fovea. (**P**) Foveal and (**Q**) perifoveal SD-OCT scans from the left eye of case 2 within the 2° by 2° square in Figure 1B, and demonstrate reasonable preservation of the IS-OS junction 250 μm inferior to fovea (**Q**) compared to the fovea (**P**). All the retinal layers are marked: ELM, external limitingmembrane; OPL, outer plexiform layer; IPL, inner plexiform layer; INL, inner nuclear layer; OS, photoreceptor outer segment; IS-OS, inner segment-outer segment junction. Photoreceptors within the *white box* on SD-OCT fall within the region scanned by AOSLO.

to the fovea (Fig. 1P). Hence, the cone mosaic appears to be less severely affected in case 2 (Fig. 4A), than in cases 6 and 7 (Figs. 4E, 4F). In case 7, the AOSLO image obtained outside the region of optical hyporeflectivity also shows a sparse distribution of wave guiding cones (Fig. 4G).

Genetic Results

All seven cases carried two validated pathogenic mutations in *KCNV2*, three of which were novel (two stop mutations: p.Glu80X and p.Gln223X; one frame-shifting insertion: p.Asp154Ala fsx58). Six cases harbored homozygous pathogenic changes; case 5 is a compound heterozygote. The ethnicity, mutation results, the protein domain involved, and details of segregation analysis and control screening are shown in Table 3.

Although characteristic ERG changes were noted in all cases, no other phenotype–genotype correlation was observed. Three cases with missense (p.Gly461Arg) or inframe deletion (p.Asp339_Val341Del) had similar visual acuities compared to three with nonsense changes (p.Asp154Ala fsx58 and p.Glu80X) at a mean age of 12.33 and 13 years, respectively (mean acuity for both groups = 20/160; 0.92 logMAR). Although all cases had disruptions in the neurosensory retina, the most preserved retinal structural integrity and the thickest central subfoveal region were noted in case 4 (p.Glu80X). The Goldmann visual field was normal at 11 years in case 1 (p.Asp154Ala fsx58); whereas, case 6 at 9 years (p.Gly461Arg) demonstrated a central 25° scotoma. Of the two cases with near-normal LA2.29 ERG a-wave amplitudes, one each had missense and nonsense mutations (cases 2 and 3, respectively). A severe flicker delay of $\geq$8 ms was found in all except case 2 (age at testing: 16 years; p.Gly461Arg). The AOSLO imaging showed marked abnormality in the cone mosaic in all subjects, but case 3 (p.Glu80X at 15 years) had a better cone mosaic than case 7 (p.Asp339_Val341 Del at 17 years) at a similar eccentricity ($\sim$4° temporal to the fovea; Figs. 4B, 4G). Cases 2 and 6 with identical missense changes (p.Gly461Arg; 18 and 9 years, respectively) had no demonstrable nystagmus at the latest visit; only case 6 showed an optical hyporeflectivity at the fovea and hence had a more disrupted cone mosaic compared with Case 2.

Discussion

This is a comprehensive study of the phenotypic characteristics of *KCNV2*-related CDSR, and to our knowledge, it is the first documentation of macular cone photoreceptor mosaic disruption in the disease. The AOSLO images obtained within the macula show individual or groupings of wave-guiding cones surrounded by areas of undetectable cones; these changes were ubiquitous regardless of genotype. The study proves rod photoreceptor sensitivity to be largely preserved in CDSR. Our results are consistent with prior studies that suggest strict genotype–ERG phenotype correlation in CDSR.[3–8,10,36]

Nyctalopia and early onset photophobia were common at presentation as previously reported.[2,5,8] Nystagmus was more common in this series as all subjects presented at a young age. Spontaneous improvement in head shaking was observed in two cases; one of them showed simultaneous improvement in nystagmus. Khan et al.[6] first reported this phenomenon of

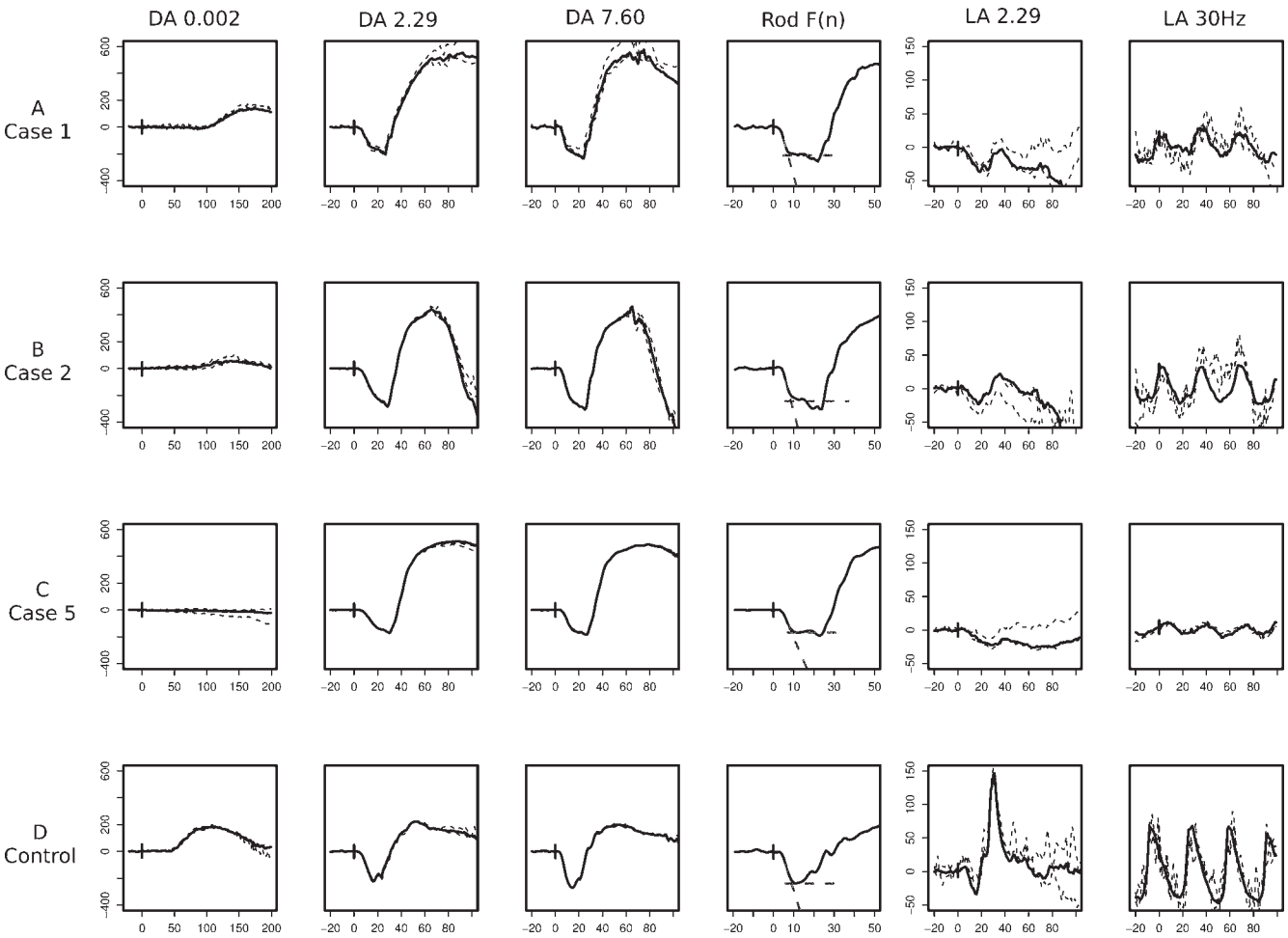

Figure 2. ERG features in three representative cases (**A**–**C**) and a control subject (**D**). For DA0.002, DA2.29, DA7.60, LA2.29, and LA30Hz ERGs, averaged waveforms are shown as *continuous lines* and individual traces are shown as *broken lines*. The dim-light scotopic ERG (DA0.002) was either nonrecordable (**C**) or markedly delayed (**A**, **B**). The DA2.29 ERG showed a late squaring of the a-wave in all three cases; the b-wave onset was delayed but b-wave amplitudes were high/supernormal. The DA7.6 ERG showed more prominent rod a-wave squaring. Rod photoreceptor function [Rod F(n)] ERGs were derived waveforms obtained after digitally subtracting LA240 ERG from DA240 ERG (see Methods section on electroretinography for details). The fitting of the slope to the steepest part of the a-wave used to calculate t_{Amax} and A_{max} are shown using *dashed lines*. Note that t_{Amax} is normal in all three cases. The cone ERGs (LA 2.29 and LA30Hz) were subnormal and delayed in the three cases. The timing of stimulus onset is marked on each figure. The *x*-axis represents timing in milliseconds and *y*-axis represents amplitude in microvolts.

spontaneous improvement of head shaking in CDSR. Head shaking is a recognized association of some forms of congenital nystagmus known to provide visual benefit.[37–39] Hence, head shaking may provide some visual benefit in cases of CDSR that manifest nystagmus. BCVA was affected early, but progressive worsening was noted only in 30% of cases. This is in keeping with literature that suggests CDSR to be a slowly progressive condition.[5] The RPE changes were limited to the macula as reported previously.[2–5,8] A peri- or parafoveal ring of hyperfluorescence was the most common FAF abnormality seen, as earlier reported in CDSR[5,28] and other cone–rod dystrophies.[40,41]

The mean central retinal thickness was reduced in CDSR as described earlier.[28] The SD-OCT demonstrated varied levels of discontinuity and disruption of the IS-OS junction and the OS layer in all eyes. Complete disruption of the IS-OS junction and OS or presence of an optical gap in the neurosensory retina, representative of a severe structural abnormality at the fovea, was noted in three cases.[28] None of the subjects in this series had involvement of RPE.[28] Foveal hypoplasia, a developmental anomaly noted in one case in our series represents a novel finding in CDSR. The etiology of its origin in the context of the genetic defect noted remains to be elucidated. Overall, the SD-OCT changes observed in CDSR are nonspecific, and similar changes have been described in achromatopsia, cone dystrophy, cone–rod dystrophy, and *ABCA4*-related disease.[42–45]

The rod b-wave to low flash strength (DA 0.002) was nonrecordable or markedly delayed; rod b-wave to DA2.29 ERG was high or supernormal as previously reported.[5] Disproportionately large increments in rod b-wave amplitude with small increments in flash strengths (across the range tested) were evident only in a subset; an insufficient number of intermediate strength flashes likely precluded observance of the same in the rest. This phenomenon is thought to be consequent on a "gated" mechanism exerted by mutated channel in the initiation of post-transduction reaction, which requires an abnormally high stimulus threshold to activate.[5] The onset of the rod b-wave was delayed at all tested flash strengths. The late squaring of the rod a-wave was a constant feature at higher flash strengths ($\geq$2.29 cd·s/m^2); the cause for this is unclear. Rod photoreceptor sensitivity (t_{Amax}) was normal, but its maximal response was reduced (A_{max}). This suggests a reduction in the number of functional rods that appear to phototransduct normally in CDSR. The delay in rod b-wave

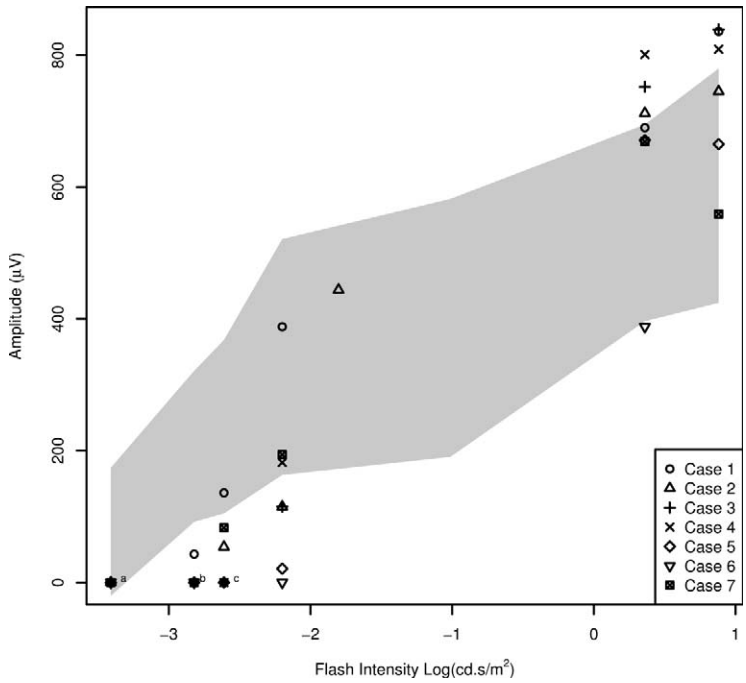

Figure 3. Scatter plot of rod b-wave amplitude across a dark-adapted intensity series (between DA0.0004 [−3.41 log units] and DA7.60 [+0.88 log units]) in the seven cases. Rod b-wave amplitudes in cases 1 and 2 showed disproportionate increments across the intensity series compared to control participants (*shaded area*). In cases 3, 4, 5, and 7, the rod b-wave was nonrecordable or subnormal at lower stimulus intensities (until DA0.002), but became high normal or supernormal at DA2.29. In case 6 (*inverted triangle*), the ERG was performed under sevofluorane anesthesia and fell within the normal range for control data under anesthetic conditions. The rod b-wave tended to saturate at a higher intensity (DA7.6) in all except cases 1 and 3. The marking "a" represents all seven cases; "b" represents cases 3, 5, 6, and 7; and "c" represents cases 3, 4, 5, and 6.

onset is consistent with a post-phototransduction locus of the defect in the rod system. Our results are similar to those of Hood et al.[9] who studied five cases of CDSR (unknown molecular basis) using a rod-isolating protocol. The *KCNV2* mRNA has been identified in human rod and cone inner segments, supporting the concept of posttransductional loci of dysfunction.[10] The cone ERGs were delayed and subnormal, consistent with the generalized "cone dystrophy" aspect of the disorder. Although, cone system abnormalities are also post-phototransduction,[9] no inappropriate increments were noted in cone b-wave amplitudes over an intensity series.[9] Also, the cone receptor maximal amplitude is known to be affected to a greater extent compared with that of the rods.[9] It is intriguing to note that the same genetic defect perhaps affects the rod and cone systems in a different manner, to a different extent, or both. No definite worsening in ERG parameters was noted during the period of this study. Two prior reports suggest mild progression in rod or cone ERG abnormalities in a few cases (5–12 year period).[5,7] Sevofluorane anesthesia may have influenced the ERG results in the lone case tested; previous studies suggest some intra- and postoperative ERG changes in animals and humans, respectively.[46,47]

The AOSLO images demonstrated a vastly disrupted macular cone photoreceptor mosaic in CDSR. The presence of discernible wave-guiding photoreceptors within 1° of the fovea supports the presumption that these photoreceptors are cones. In this study, the authors performed manual counting of presumed cones to estimate densities; it is possible that not all cones were visualized during the process. Others have calculated cone spacings from the Fourier transform of the images,[17] but this was not possible because of abnormal, irregular spacing of the cones. The resulting cone-density estimates were much lower than in young adults with normal visual development at similar eccentricities.[48,49] In all cases, individual or groups of wave-guiding cones were surrounded by patches in which cones were either absent or did not reflect light out of the eye. The extent of macular cone mosaic disruption was more severe compared with cone dysfunction syndromes like achromatopsia and oligocone trichromacy.[22–24] In cases with minimal or no nystagmus, permitting better imaging closer to fovea, the degree of perifoveal cone photoreceptor disruption was consistent with the extent of photoreceptor IS-OS junction disruption noted on SD-OCT. Previous studies have consistently reported reasonable correlation between IS-OS junction disruption and absence of visible cones at the fovea and perifovea in cone dysfunction syndromes[23,24] and a wide range of retinal conditions.[27,50,51] Further, the cone mosaic and density were also markedly abnormal in regions outside the fovea where SD-OCT showed less marked IS-OS disruption; the presence of intact rod photoreceptors in the region is the likely reason for this relative IS-OS preservation.[52] The presence of a generalized cone abnormality in the ERG suggests that regions of nondetectable cones on AOSLO might represent dysfunctional or absent cones rather than cones that are functional but not visible.

Two pathogenic *KCNV2* mutations were identified in all cases, signifying the specificity of characteristic ERG changes observed.[3–8,10,36] Three novel mutations were identified (p.Glu80X, p.Gln223X, and p.Asp154Ala fsx58). These changes would likely succumb to nonsense-mediated decay of mRNA. Even if translated, the resultant protein would be severely truncated and nonfunctional because it would lack all six transmembrane domains and the pore loop of the channel. The p.Gly461Arg was the most common mutation found in this study and in the literature.[3,4,7,8,28] This missense change involves the third amino acid of the highly conserved GlyTyrGly tripeptide K^+ selective motif of the pore loop in

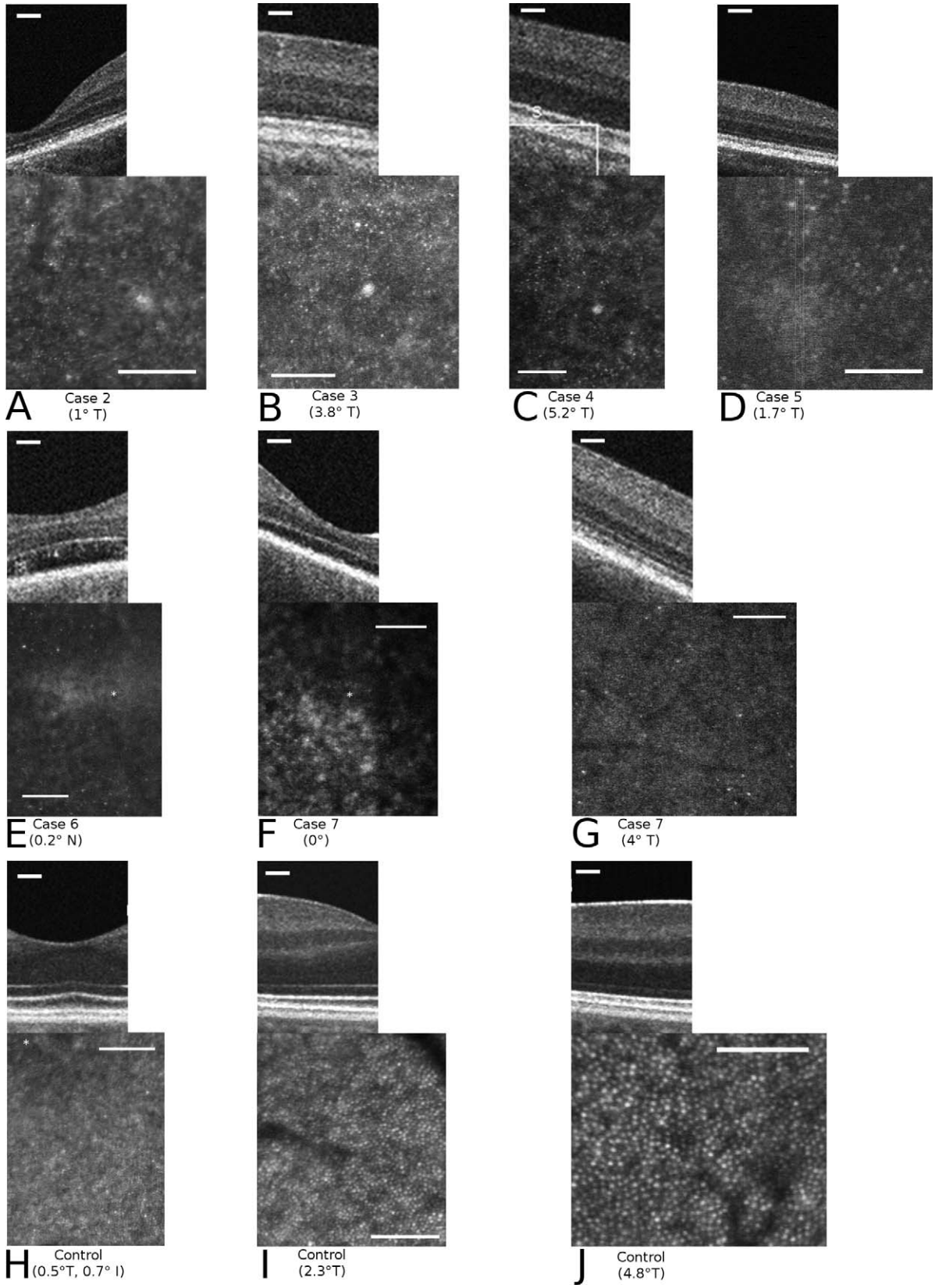

Figure 4. (**A–G**) Macular cone photoreceptor morphology in six cases. The AOSLO images are shown for subsections of 2° by 2° fields, centered on the horizontal meridian, below a 2° horizontal section of SD-OCT that overlaps the region scanned by the AOSLO. The AOSLO images from similar eccentricities in a control subject are also provided (**H–J**). Each AO image is cropped from the original 2° by 2° frames to include regions in most focus. *Horizontal bars* on each of the AOSLO and SD-OCT images represent 0.4°. The approximate horizontal center of each AOSLO image is labeled, except for the control image (**H**), which also has an inferior offset. N, T, and I represent nasal, temporal, and inferior, respectively. The cone mosaic was grossly disrupted in every case. Single or groupings of wave guiding cones surrounded by regions of absent or nondetectable cones

composed the pattern observed in all areas. Cases 6 and 7, which showed an optical gap at the fovea on SD-OCT, also demonstrated severe disruption of the perifoveal cone mosaic (**E**, **F**, respectively; fovea marked as *white asterisks*). In case 5, there is additional image blur due to the presence of nystagmus and the retinal location is estimated.

Table 3. Details and Analysis of Genetic Results in KCNV2 in the Seven Affected Cases

Case	Ethnicity	Nucleotide and Protein Alteration	Protein Domain	Mutation Status	Segregation and Validation of the Novel Changes
1	Iranian/ consanguinity	c.460_461insCG*: p.Asp154Ala fsx58	Cytoplasmic N terminal A and B box	Novel	Both parents heterozygous for c.461insCG. Control screening ($n = 300$, 84 were ethnic specific) using restriction enzyme digest.
2	Caucasian	c.1381G > A*: p.Gly461Arg	Pore loop	Reported[3,4,6,8,28]	Dad is heterozygous for c.1381G > A. Mom not tested.
3, 4†	Palestinian/ consanguinity	c.238G > T*: p.Glu80Stop	Extracellular	Novel	Mom is heterozygous for c.238G > T. Control screen ($n = 300$, 80 were ethnic specific) using ARMS assay; p.Glu80Asp earlier reported to be pathogenic.[7]
5	Chinese	c.667C > T /c.1381G > A: p.Gln223Stop/p.Gly461Arg	Extracellular and pore loop	c.667C > T is novel	Dad heterozygous for c.667C > T; mom heterozygous for c.1381G > A. Control screening for c.667C > T ($n = 300$, 186 were ethnic specific) using ARMS assay.
6	Caucasian	c.1381G > A*: p.Gly461Arg	Pore loop	Reported[3,4,6,8,28]	Not performed
7	Caucasian	c.1015_1025DelACCTGGTGG*: p.Asp339_Val341Del	Transmembrane domain S3	Reported[4,10,44]	Not performed

ARMS, amplification refractory mutation system.
* Indicates homozygous state.
† Cases 3 and 4 are siblings.

KCNV2, which interacts with other K^+ channel subunits to form the ion-selective pore.[11,13] The first two amino acids of the previously reported p.Asp339_Val341Del mutation are known to be highly conserved in 13 vertebrate orthologous channels.[11] No notable genotype–phenotype correlation was observed in this study. A previous study noted slightly better BCVA in cases with homozygous p.Gly461Arg mutations compared with those carrying two nonsense alleles.[4]

To summarize, this study has refined and extended the phenotypic description in *KCNV2*-related CDSR. The disease is slowly progressive with predominant worsening in central vision parameters. Structural retinal and lipofuscin accumulation abnormalities are commonly present and help monitor severity, but are not specific to the disease. The ERG changes are diagnostic of CDSR and facilitate identification of underlying genetic defect; the sensitivity of the functioning rod system appears to be normal. Macular cone photoreceptor mosaic is markedly disrupted in CDSR. With emerging treatment success in human and animal models of retinal dystrophies using various modalities,[53–56] in vivo monitoring of photoreceptors could be a useful adjunct to monitor outcome[57]; hence, knowledge of baseline cone photoreceptor morphology in CDSR is useful. Some groups have recently imaged rods using AOSLO,[58–60] and in future, this information could provide additional insight into the disease.

Acknowledgments

The authors acknowledge the contribution of colleagues at Hospital for Sick Children for appropriate assistance: Cynthia VandenHoven and Cory Brake (Imaging), Megan Day, and Joanne Sutherland (Genetic counselling), Carole Panton and Melissa Cotesta (Electrophysiology), and Gail Billingsley and Nicole Forster (Héon Lab, Genetics and Genome Biology). The authors thank Daniel Hammer and Daniel Ferguson (Physical Sciences, Inc., Andover, MA) for assistance in AOSLO imaging. Software for aligning AOSLO images was courtesy of Alf Dubra, Medical College of Wisconsin.

References

1. Gouras P, Eggers HM, MacKay CJ. Cone dystrophy, nyctalopia, and supernormal rod responses. A new retinal degeneration. *Arch Ophthalmol*. 1983;101:718–724.
2. Michaelides M, Holder GE, Webster AR, et al. A detailed phenotypic study of "cone dystrophy with supernormal rod ERG." *Br J Ophthalmol*. 2005;89:332–339.
3. Thiagalingam S, McGee TL, Weleber RG, et al. Novel mutations in the KCNV2 gene in patients with cone dystrophy and a supernormal rod electroretinogram. *Ophthalmic Genet*. 2007; 28:135–142.

4. Wissinger B, Dangel S, Jagle H, et al. Cone dystrophy with supernormal rod response is strictly associated with mutations in KCNV2. *Invest Ophthalmol Vis Sci*. 2008;49:751–757.
5. Robson AG, Webster AR, Michaelides M, et al. "Cone dystrophy with supernormal rod electroretinogram": a comprehensive genotype/phenotype study including fundus autofluorescence and extensive electrophysiology. *Retina*. 2010; 30:51–62.
6. Khan AO, Alrashed M, Alkuraya FS. 'Cone dystrophy with supranormal rod response' in children. *Br J Ophthalmol*. 2012;96:422–426.
7. Friedburg C, Wissinger B, Schambeck M, Bonin M, Kohl S, Lorenz B. Long-term follow-up of the human phenotype in three siblings with cone dystrophy associated with a homozygous p.G461R mutation of KCNV2. *Invest Ophthalmol Vis Sci*. 2011;52:8621–8629.
8. Ben Salah S, Kamei S, Senechal A, et al. Novel KCNV2 mutations in cone dystrophy with supernormal rod electroretinogram. *Am J Ophthalmol*. 2008;145:1099–1106.
9. Hood DC, Cideciyan AV, Halevy DA, Jacobson SG. Sites of disease action in a retinal dystrophy with supernormal and delayed rod electroretinogram b-waves. *Vision Res*. 1996;36: 889–901.
10. Wu H, Cowing JA, Michaelides M, et al. Mutations in the gene KCNV2 encoding a voltage-gated potassium channel subunit cause "cone dystrophy with supernormal rod electroretinogram" in humans. *Am J Hum Genet*. 2006;79:574–579.
11. Ottschytsch N, Raes A, Van Hoorick D, Snyders DJ. Obligatory heterotetramerization of three previously uncharacterized Kv channel alpha-subunits identified in the human genome. *Proc Natl Acad Sci U S A*. 2002;99:7986–7991.
12. Shealy RT, Murphy AD, Ramarathnam R, Jakobsson E, Subramaniam S. Sequence-function analysis of the K+-selective family of ion channels using a comprehensive alignment and the KcsA channel structure. *Biophys J*. 2003;84:2929–2942.
13. Czirjak G, Toth ZE, Enyedi P. Characterization of the heteromeric potassium channel formed by kv2.1 and the retinal subunit kv8.2 in Xenopus oocytes. *J Neurophysiol*. 2007;98:1213–1222.
14. Roorda A, Williams DR. The arrangement of the three cone classes in the living human eye. *Nature*. 1999;397:520–522.
15. Liang J, Williams DR, Miller DT. Supernormal vision and high-resolution retinal imaging through adaptive optics. *J Opt Soc Am A Opt Image Sci Vis*. 1997;14:2884–2892.
16. Brainard DH, Roorda A, Yamauchi Y, et al. Functional consequences of the relative numbers of L and M cones. *J Opt Soc Am A Opt Image Sci Vis*. 2000;17:607–614.
17. Roorda A, Romero-Borja F, Donnelly Iii W, Queener H, Hebert T, Campbell M. Adaptive optics scanning laser ophthalmoscopy. *Opt Express*. 2002;10:405–412.
18. Hofer H, Carroll J, Neitz J, Neitz M, Williams DR. Organization of the human trichromatic cone mosaic. *J Neurosci*. 2005;25: 9669–9679.
19. Roorda A, Williams DR. Optical fiber properties of individual human cones. *J Vis*. 2002;2:404–412.
20. Wojtkowski M, Bajraszewski T, Gorczynska I, et al. Ophthalmic imaging by spectral optical coherence tomography. *Am J Ophthalmol*. 2004;138:412–419.
21. Wojtkowski M, Srinivasan V, Fujimoto JG, et al. Three-dimensional retinal imaging with high-speed ultrahigh-resolution optical coherence tomography. *Ophthalmology*. 2005; 112:1734–1746.
22. Carroll J, Choi SS, Williams DR. In vivo imaging of the photoreceptor mosaic of a rod monochromat. *Vision Res*. 2008;48:2564–2568.
23. Genead MA, Fishman GA, Rha J, et al. Photoreceptor structure and function in patients with congenital achromatopsia. *Invest Ophthalmol Vis Sci*. 2011;52:7298–7308.
24. Michaelides M, Rha J, Dees EW, et al. Integrity of the cone photoreceptor mosaic in oligocone trichromacy. *Invest Ophthalmol Vis Sci*. 2011;52:4757–4764.
25. Duncan JL, Talcott KE, Ratnam K, et al. Cone structure in retinal degeneration associated with mutations in the peripherin/RDS gene. *Invest Ophthalmol Vis Sci*. 2011;52:1557–1566.
26. Duncan JL, Ratnam K, Birch DG, et al. Abnormal cone structure in foveal schisis cavities in X-linked retinoschisis from mutations in exon 6 of the RS1 gene. *Invest Ophthalmol Vis Sci*. 2011;52:9614–9623.
27. Chen Y, Ratnam K, Sundquist SM, et al. Cone photoreceptor abnormalities correlate with vision loss in patients with Stargardt disease. *Invest Ophthalmol Vis Sci*. 2011;52:3281–3292.
28. Sergouniotis PI, Holder GE, Robson AG, Michaelides M, Webster AR, Moore AT. High-resolution optical coherence tomography imaging in KCNV2 retinopathy. *Br J Ophthalmol*. 2012;96:213–217.
29. Marmor MF, Fulton AB, Holder GE, Miyake Y, Brigell M, Bach M. ISCEV Standard for full-field clinical electroretinography (2008 update). *Doc Ophthalmol*. 2009;118:69–77.
30. Marmor MF, Holder GE, Seeliger MW, Yamamoto S. Standard for clinical electroretinography (2004 update). *Doc Ophthalmol*. 2004;108:107–114.
31. Hood DC, Birch DG. Assessing abnormal rod photoreceptor activity with the a-wave of the electroretinogram: applications and methods. *Doc Ophthalmol*. 1996;92:253–267.
32. Nilsson J, Wright T, Westall CA. Rod a-wave analysis using high intensity flashes adds information on rod system function in 25% of clinical ERG recordings. *Vision Res*. 2008;48:1920–1925.
33. Heckenlively JR, Arden GB. *Principles and Practice of Clinical Electrophsyiology of Vision*. 2nd ed. Cambridge, MA: MIT Press; 2006.
34. Thevenaz P, Ruttimann UE, Unser M. A pyramid approach to subpixel registration based on intensity. *IEEE Trans Image Process*. 1998;7:27–41.
35. Muraishi H. Fundamental of medical image processing with personal computer system—development of Plugins by ImageJ [in Japanese]. *Nihon Hoshasen Gijutsu Gakkai Zasshi*. 2010;66:260–264.
36. Wissinger B, Schaich S, Baumann B, et al. Large deletions of the KCNV2 gene are common in patients with cone dystrophy with supernormal rod response. *Hum Mutat*. 2011;32:1398–1406.
37. Gresty MA, Halmagyi GM. Abnormal head movements. *J Neurol Neurosurg Psychiatry*. 1979;42:705–714.
38. Gottlob I, Zubcov AA, Wizov SS, Reinecke RD. Head nodding is compensatory in spasmus nutans. *Ophthalmology*. 1992;99: 1024–1031.
39. Carl JR, Optican LM, Chu FC, Zee DS. Head shaking and vestibulo-ocular reflex in congenital nystagmus. *Invest Ophthalmol Vis Sci*. 1985;26:1043–1050.
40. Downes SM, Payne AM, Kelsell RE, et al. Autosomal dominant cone-rod dystrophy with mutations in the guanylate cyclase 2D gene encoding retinal guanylate cyclase-1. *Arch Ophthalmol*. 2001;119:1667–1673.
41. Robson AG, Michaelides M, Saihan Z, et al. Functional characteristics of patients with retinal dystrophy that manifest abnormal parafoveal annuli of high density fundus autofluorescence; a review and update. *Doc Ophthalmol*. 2008;116: 79–89.
42. Thomas MG, Kumar A, Kohl S, Proudlock FA, Gottlob I. High-resolution in vivo imaging in achromatopsia. *Ophthalmology*. 2011;118:882–887.
43. Birch DG, Wen Y, Locke K, Hood DC. Rod sensitivity, cone sensitivity, and photoreceptor layer thickness in retinal

degenerative diseases. *Invest Ophthalmol Vis Sci*. 2011;52:7141–7147.

44. Burke TR, Tsang SH. Allelic and phenotypic heterogeneity in ABCA4 mutations. *Ophthalmic Genet*. 2011;32:165–174.
45. Yokochi M, Li D, Horiguchi M, Kishi S. Inverse pattern of photoreceptor abnormalities in retinitis pigmentosa and cone-rod dystrophy. *Doc Ophthalmol*. 2012;125:211–218.
46. Yanase J, Ogawa H. Effects of halothane and sevoflurane on the electroretinogram of dogs. *Am J Vet Res*. 1997;58:904–909.
47. Iohom G, Whyte A, Flynn T, O'Connor G, Shorten G. Postoperative changes in the full-field electroretinogram following sevoflurane anaesthesia. *Eur J Anaesthesiol*. 2004;21:272–278.
48. Song H, Chui TY, Zhong Z, Elsner AE, Burns SA. Variation of cone photoreceptor packing density with retinal eccentricity and age. *Invest Ophthalmol Vis Sci*. 2011;52:7376–7384.
49. Chui TY, Song H, Burns SA. Individual variations in human cone photoreceptor packing density: variations with refractive error. *Invest Ophthalmol Vis Sci*. 2008;49:4679–4687.
50. Ratnam K, Vastinsalo H, Roorda A, Sankila EM, Duncan JL. Cone structure in patients with Usher syndrome type III and mutations in the Clarin 1 gene. *Arch Ophthalmol*. 2013;131:67–74.
51. Ooto S, Hangai M, Takayama K, et al. High-resolution photoreceptor imaging in idiopathic macular telangiectasia type 2 using adaptive optics scanning laser ophthalmoscopy. *Invest Ophthalmol Vis Sci*. 2011;52:5541–5550.
52. Hood DC, Zhang X, Ramachandran R, et al. The inner segment/outer segment border seen on optical coherence tomography is less intense in patients with diminished cone function. *Invest Ophthalmol Vis Sci*. 2011;52:9703–9709.
53. Bainbridge JW, Smith AJ, Barker SS, et al. Effect of gene therapy on visual function in Leber's congenital amaurosis. *N Engl J Med*. 2008;358:2231–2239.
54. Maguire AM, Simonelli F, Pierce EA, et al. Safety and efficacy of gene transfer for Leber's congenital amaurosis. *N Engl J Med*. 2008;358:2240–2248.
55. Lu B, Malcuit C, Wang S, et al. Long-term safety and function of RPE from human embryonic stem cells in preclinical models of macular degeneration. *Stem Cells*. 2009;27:2126–2135.
56. Li Y, Tao W, Luo L, et al. CNTF induces regeneration of cone outer segments in a rat model of retinal degeneration. *PLoS One*. 2010;5:e9495.
57. Talcott KE, Ratnam K, Sundquist SM, et al. Longitudinal study of cone photoreceptors during retinal degeneration and in response to ciliary neurotrophic factor treatment. *Invest Ophthalmol Vis Sci*. 2011;52:2219–2226.
58. Doble N, Choi SS, Codona JL, Christou J, Enoch JM, Williams DR. In vivo imaging of the human rod photoreceptor mosaic. *Opt Lett*. 2011;36:31–33.
59. Dubra A, Sulai Y, Norris JL, et al. Noninvasive imaging of the human rod photoreceptor mosaic using a confocal adaptive optics scanning ophthalmoscope. *Biomed Opt Express*. 2011;2:1864–1876.
60. Merino D, Duncan JL, Tiruveedhula P, Roorda A. Observation of cone and rod photoreceptors in normal subjects and patients using a new generation adaptive optics scanning laser ophthalmoscope. *Biomed Opt Express*. 2011;2:2189–2201.